ISSN 1075-7015, Geology of Ore Deposits, 2025, Vol. 67, No. 2, pp. 129–142. © Pleiades Publishing, Ltd., 2025.

"Invisible" Gold and Other Impurity Elements in Pyrite and Arsenopyrite from the Mayskoe Deposit (Chukotka)

N. V. Sidorova[a, *], A. V. Volkov[a, **], E. E. Tyukova[a, b], E. N. Kaigorodova[a], E. V. Koval'chuk[a, c], and E. A. Minervina[a]

[a] *Institute of Geology of Ore Deposits, Petrography, Mineralogy, and Geochemistry, Russian Academy of Sciences, Moscow, 119017 Russia*

[b] *Scientific Geoinformation Center, Russian Academy of Sciences, Moscow, 119091 Russia*

[c] *Sergo Ordzhonikidze Russian State University for Geological Prospecting, Moscow, 117997 Russia*

**e-mail: nsidorova989@mail.ru*

***e-mail: tma2105@mail.ru*

Received August 8, 2024; revised October 28, 2024; accepted November 1, 2024

Abstract—The gold-bearing sulphides (pyrite and arsenopyrite) from disseminated refractory ores of the Mayskoe gold deposit (Central Chukotka) were studied using modern precision methods (electron microprobe analysis and laser ablation-inductively coupled plasma-mass spectrometry). The distribution patterns of macro elements (As, Fe, S), as well as trace elements (Ni, Zn, Sb, Co, Cu, Ag), in pyrite and arsenopyrite, including the content of "invisible" Au and its correlation with other elements were studied. Based on recieved data, the sequence of crystallization and the relationships of gold-bearing sulphides at the main and most productive gold–sulphide stage of the deposite formation were established.

Keywords: Chukotka, Mayskoe deposit, pyrite, arsenopyrite, "invisible" gold, EMPA, laser ablation-inductively coupled plasma-mass spectrometry

DOI: 10.1134/S1075701524600762

INTRODUCTION

The Mayskoe gold deposit (Chukotka), along with such deposits as Olympiada and Veduga (Krasnoyarsk region), Nezhdaninskoe and Kyuchus (Yakutia), and Albazino (Khabarovsk region), is one of the most famous gold deposits in Russia containing gold in a dispersed form mainly or predominantly in sulphides (so-called "invisible" gold) (Volkov and Sidorov, 2007). The study of gold-bearing sulphides in these deposits is relevant from both a scientific and practical point of view. The presence of invisible gold in sulphides gives the ores refractory properties and so data on the distribution of such gold in individual minerals are valuable for developing ore-treatment processes. Studying the distribution of trace elements in gold-bearing sulphides that form commercial accumulations can supplement the known information about the formation conditions of such unique ore objects.

Gold-bearing sulphides of disseminated ores of the Mayskoe deposit, especially fine-acicular arsenopyrite, attracted the attention of many researchers, A.M. Gavrilov being the first one (Central Research Institute of Geological Prospecting for Base and Precious Metals (TsNIGRI)). A.M. Gavrilov and A.P. Pleshakov (Gavrilov et al., 1982) revealed an irregular, dense cluster of rounded gold inclusions (0.04–0.3 μm) in arsenopyrite using scanning electron microscopy and electrone microanalysis methods. It was found that finely dispersed gold is distributed throughout the entire volume of arsenopyrite grains. According to atomic absorption and neutron activation analyses, the average Au content in arsenopyrite was 620 ppm, and in pyrite it was 40 ppm (Novozhilov and Gavrilov, 1999).

In addition, the study of gold-bearing sulphides from the Mayskoe deposit were carried out by researchers of Moscow State University under the direction of M.S. Sakharova. The results obtained are discussed in detail in the monograph (Shilo et al., 1992). Geochemical features of sulphides were studied by laser microspectral analysis of monomineral fractions. According to the authors' data, the maximum gold content in arsenopyrite is 500 ppm. In pyrite, maximum gold content (up to 156 ppm) was noted in rounded sedimentary–diagenetic varieties.

Small gold particles of rounded and isometric shape up to 6 μm in size, which are characterized by increased emission of secondary electrons, were identified using scanning electron microscope on the surface of crystals of fine crystalline arsenopyrite and, to a lesser extent, pyrite. This phenomenon is characteristic for native chemical elements with high average

atomic numbers (Au, Ag, Pt). According to this, as well as to the similarity of the studied particles with the morphology of visible gold, it was assumed that these are particles of finely dispersed gold (Shilo et al., 1992).

In (Bortnikov et al., 2004), the results of EMPA and atomic absorption study of pyrite and arsenopyrite from the quartz-pyrite-arsenopyrite mineral association with finely dispersed gold of the Mayskoe deposit are presented. According to EMPA data, S/As ratio in elongated-prismatic arsenopyrite ranges from 1.054 to 1.482; gold content reaches 1.2 wt %. Up to 6.5 wt % As and up to 0.4 wt % Au were measured in pyrite. According to atomic absorption spectroscopy (AAS) data, the gold content is 182.4–1030 ppm in arsenopyrite and 1.44–42.74 ppm in pyrite. The authors of (Bortnikov et al., 2004) noted that no native gold was found in arsenopyrite grains with maximum gold content under microscopic studies.

According to (Volkov et al., 2007), it was determined by the EMPA method that the gold content in arsenopyrite from samples of disseminated ores of the Mayskoe deposit varies from 0 to 1100 ppm (320 ppm average for 10 grains). According to neutron-activation analysis data, gold content varies from 300 to 1975 ppm. The authors also noted that arsenopyrite with the highest S–As ratio has the maximum gold content. The gold content in pyrite of disseminated ores of the Mayskoe deposit was below the measurement detection limit of the electrone-microprobe micro-analysis. However, high arsenic contents were found in the rims of pyrite metacrystals.

This paper presents the results of studying gold-bearing sulphides (pyrite and arsenopyrite) of the Mayskoe deposit by EMPA method and laser ablation-inductively coupled plasma-mass spectrometry (LA-ICP-MS). The main purpose of this work was to determine typomorphic characteristics of distribution of trace elements in gold-bearing sulphides with "invisible" gold.

GEOLOGICAL SETTING AND MINERAL COMPOSITION OF THE MAYSKOE GOLD-ORE DEPOSIT

The Mayskoe deposit is located 180 km east of the city Pevek, the administrative center of Chaunsky district of the Chukotka autonomous region (Fig. 1, inset).

The deposit was discovered in 1972 as a result of a 1 : 50000 scale geological survey by S.A. Grigorov and N.M. Samorukov (Grigorov et al., 1973). Exploration of the deposit was carried out until 1982 (Novozhilov et al., 1983). The Mayskoe deposit is one of the five largest gold deposits in Russia in terms of reserves. In 2009, it was acquired by Polymetal Co. Since 2010, an underground mine has been operating at the deposit, and since 2016-an open pit. A flotation plant with a capacity of 850 thousand tons per year came into operation in 2013. According to the data available (www.polymetal.ru), the reserves and resources of the deposit are 155 t of gold at the end of 2021. In 2021, the mine produced 4.3 t of gold.

The refractory ores of the Mayskoe deposit are processed by flotation to produce gold-bearing sulphide concentrate, which is then transported by sea to the Amur Metallurgical Plant to extract gold by autoclave oxidation and cyanidation, or sold on the global market (www.polymetal.ru).

Geological Setting

The Mayskoe ore field is located within the boundaries of the Kukeney Satellite Intrusive Dome Structure (IDS) located in the central part of the Chukotka folded system of the Mesozoides at the border zone with the Okhotsk–Chukotka volcanic belt (Volkov et al., 2006). The ore field is composed of dislocated sandstone-shale rocks of Middle and Upper Triassic age, intruded by numerous dikes and subvolcanic bodies of the felsic composition and solitary Cretaceous lamprophyre dikes.

The Mayskoe deposit is confined to a daughter dome uplift within the IDS. The structure of the deposit is defined by a NE-striking horst-anticlinal fold (eroded dome) with southern dip of the hinge at an angle of 15°–20°, complicated by block motions along latitudinal and submeridional faults. Along the latter the linear dynamometamorphic zones hosting ore bodies were emplaced.

About 30% of the deposit volume is represented by dikes, which form a 3 × 3-km field of convergent subparallel bodies with general meridional strike. There are two generations of dykes that consistently followed each other: (1) granite–granodiorite porphyries, aplites, and lamprophyres and (2) subvolcanic rhyolite porphyries. The thickness of the dikes varies from the first meters to 50–60 m, their dip is predominantly southeastern, at angles of 50°–70°. Late dikes of rhyolite porphyries constitute the bulk of igneous rocks of the deposit. According to isotopic age dating (K–Ar method, Laboratory of Isotope Geochronology, Shilo North-East Interdisciplinary Scientific Research Institute, Far East Branch, Russian Academy of Sciences (NEISRI FEB RAS) (Volkov et al., 2006)), the intrusion time for dyke bodies is estimated to be boundary of Early and Late Cretaceous. In the deposit, the dyke field is accompanied by a wide development of explosive breccias, predominantly in the central part of the deposit. The breccias occur in the form of convergent branching vein-shaped bodies and extend to a depth of more than 700 m from the surface. The general strike of dikes is also submeridional, with a predominant eastern dip, at an angle of 60°–75°. The breccias are composed of fragments of all types of sedimentary rocks occurring in deposit, cemented by

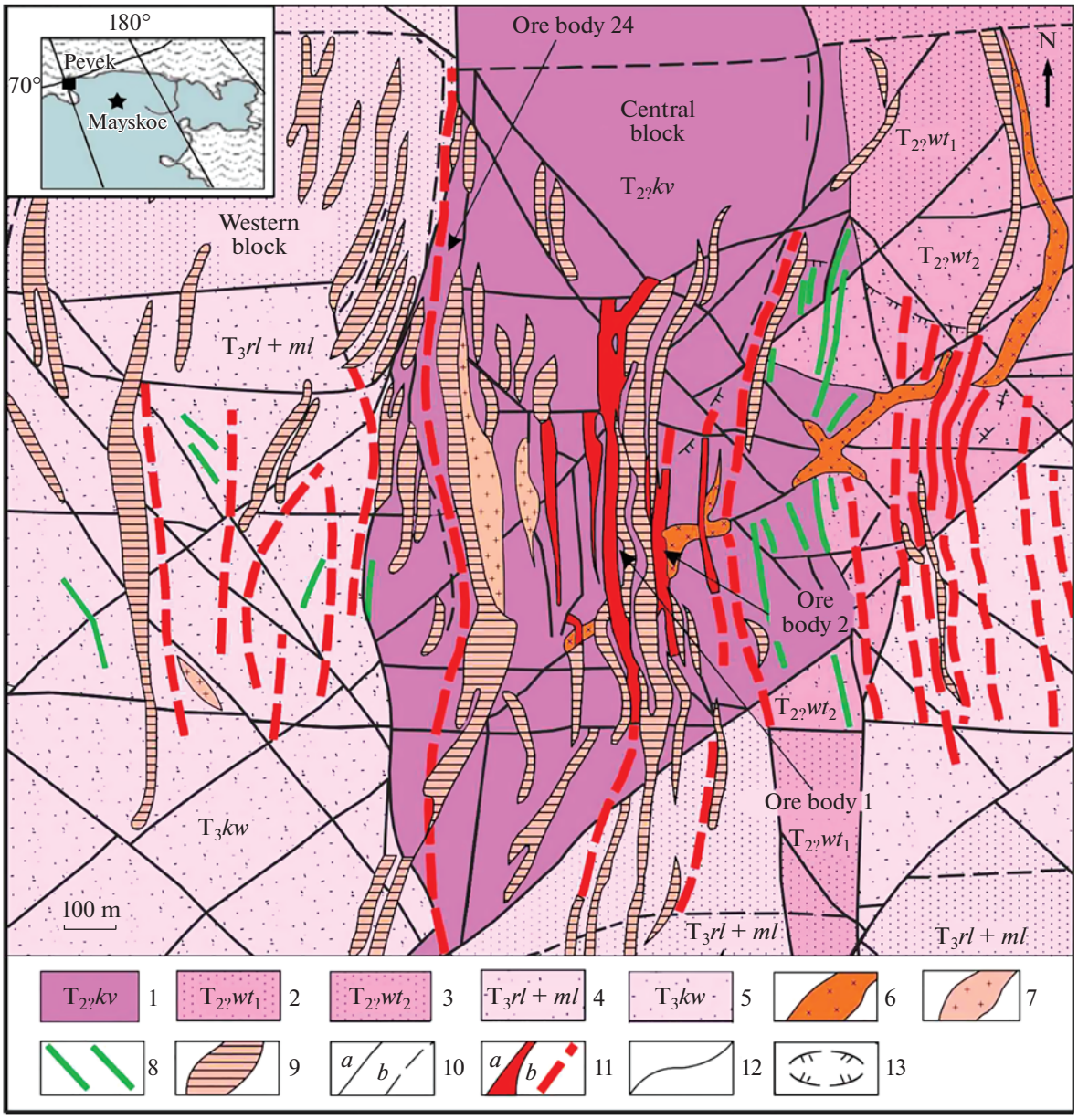

Fig. 1. Schematic geologic map of the Mayskoe deposit after (Novozhilov and Gavrilov, 1999; Volkov et al., 2006), with amendments. The geographic location of the deposit is shown in the inset. Middle Triassic: (1) siltstones of the Keveem Formation; (2) inequigranular sandstones of the Vatapvaam Formation, lower subformation; (3) inequigranular sandstones of the Vatapvaam Formation, upper subformation. Upper Triassic: (4) alternating of sandstones and siltstones of the Relkuveem and Mleluveem formations; (5) alternating of sandstones and siltstones of the Kuveemkai Formation; (6–9) Early to Late Cretaceous igneous rocks: (6) granodiorites and granite porphyries; (7) aplites; (8) lamprophyres; (9) rhyolite porphyries; (10) faults (*a*) established and (*b*) inferred; (11) ore bodies (*a*) exposed and (*b*) blind; (12) geological boundaries; (13) outline of sericite metasomatic rocks (beresites).

crushed in varying degrees fragments of the same rocks.

In the central part of the deposit, bleached metasomatic rocks of quartz–sericite composition (rarely with carbonate), classified as beresites, are widespread (Novozhilov and Gavrilov, 1999; Artemiev, 2016). The rare-metal mineralization is paragenetically associated with these rocks. The transition to unaltered rocks is gradual at a distance of 30–50 m. The metasomatic contour looks like the oval elongated in the northeastern direction and extending downward. According to (Volkov et al., 2006), gold ore bodies are located beyond the field of beresites.

More than 30 ore bodies have been identified within the deposit, 70% of which do not reach the surface. A strike length of ore bodies ranges from 200 to 1200 m. Most of them are not outlined along the dip. The average thickness of the bodies is 2 m, and the

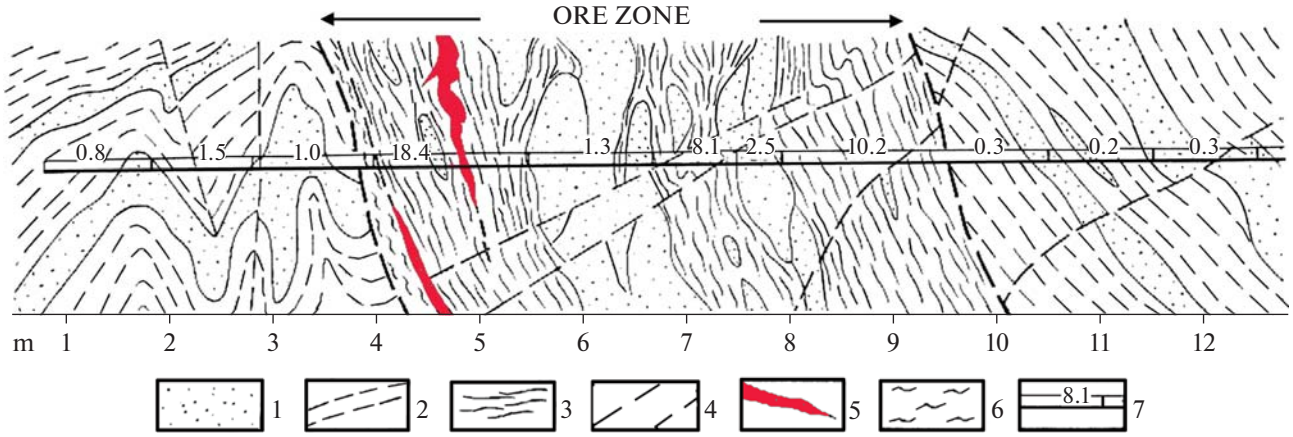

Fig. 2. The structure of the ore zone (ore body 1) of the Mayskoe deposit (Novozhilov et al., 1988): (1) fine-grained sandstones; (2) alternating of siltstones and silty clay shales; (3) intensely cleavaged siltstones with impregnated ore mineralization; (4) faults; (5) quartz–stibnite zones; (6) milonitization zones with slickensides; (7) trench-channel samples and results of gold assay test (ppm).

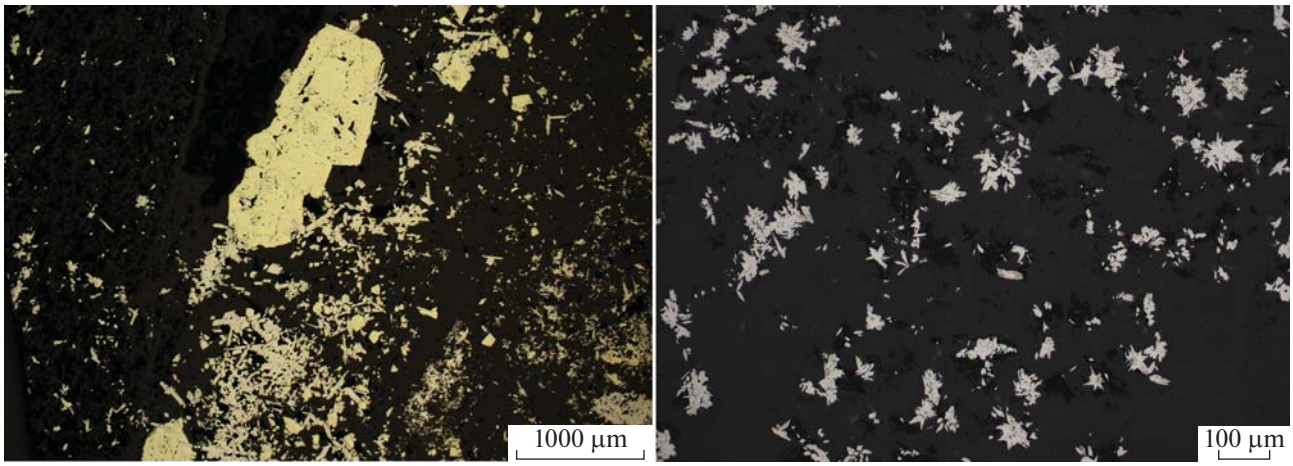

Fig. 3. Rich impregnated pyrite–arsenopyrite ore of the Mayskoe deposit, ore body 1. Reflected polarized light photomicrograph.

average gold grade is 11.5 ppm. The ore bodies have distinct geological boundaries and are represented by mineralized crushed zones. Locally, sulphidization, vein silicification, and, to a lesser extent, sericitization and kaolinization are manifested in these zones. Ore outlines are defined both by geological boundaries that fix the zones of the most dynamometamorphically transformed sulphidized rocks (Fig. 2) and by sampling data (Novozhilov et al., 1988).

The ore-bearing rocks are siltstones, clay shales, and fine-grained sandstones of the Keveem and Relkuveem–Mleluviem; less frequently those of the Vatapvaam Formation; and rarely dikes of rhyolite porphyries with fine-crystal impregnation of Au-rich sulphides (pyrite and arsenopyrite).

Mineral Composition of Ores

The mineralogy of ores of the Mayskoe deposit is discussed in detail in a number of articles (Andreev, 1984; Shilo et al., 1992; Novozhilov and Gavrilov, 1999; Bortnikov et al., 2004). It was established (Gavrilov et al., 1982, 1986) that gold at the deposit occurs both in its native form and in "invisible" form in sulphides. The bulk mass of gold in ores (up to 90%) is contained in sulphides, predominantly in arsenopyrite.

Primary ores are represented by impregnation of the smallest (tenths to hundred-thousandths of a millimeter) crystals and aggregates of Au-rich arsenopyrite and pyrite in dark, often weakly silicified sedimentary rocks (Fig. 3). There are also quartz micro veinlets containing Au-rich sulphides.

The sulphide content in impregnated ores is 6–8 vol % on average, with pyrite predominating (by from two to three times). The content of antimony in the ore reaches 0.2 wt %; the content of organic carbonaceous matter, 0.3 wt % on average; As, 1.5 wt %; and Ag, 4 ppm. Pyrite contains up to 5–7 wt % of As.

Quartz–sulphide–polymetallic and quartz–stibnite veins, veinlets, and nests are also observed within

some ore bodies, often with small impregnation of native gold. The Au content exceeds 20 ppm, the Ag content reaches 700 ppm. These ores contain coarse gold (>1 mm) with a fineness of 850–950‰.

The exposed upper part of the ore bodies of the deposit is oxidized up to a depth of 80 m. The average gold content in oxidized ores is 22 ppm. Gold grains in oxidized ores are 0.01–0.1 mm in size, fineness is 950‰ (Novozhilov and Gavrilov, 1999; Volkov et al., 2006).

According to (Andreev, 1984), the general zonal distribution of two mineral associations was established at the stage of exploration of the deposit: rare metal–polymetallic (Mo–W–Sn–Zn–Pb) and antimony with a predominant shift of rare-metal mineralization to the eastern flank of the deposit, and antimony to the western flank.

As a result of mineralogical studies performed by researchers at the TsNIGRI (Novozhilov and Gavrilov, 1999), the following scheme of ore process development at the Mayskoe deposit was proposed: (1) formation of stockwork pyrrhotite–molybdenite–quartz rare-metal mineralization associated with the plutonogenic group of dykes in the central part of the deposit, (2) formation of gold–sulphide (gold–pyrite–arsenopyrite) disseminated ores in mineralized crushing zones, (3) development of Ag-bearing quartz–polysulphide vein mineralization, and (4) formation of quartz–stibnite veins and native As mineralization.

According to the studies of the researchers of the Department of Mineralogy of Moscow State University (Bortnikov et al., 2004), it is assumed that the Mayskoe deposit was formed during the following three stages: (1) gold–sulphide with disseminated pyrite–arsenopyrite association with "invisible" gold; (2) rare metal, with quartz–molybdenite and quartz–wolframite association and sulphides (galena, sphalerite, Pb and Cu sulphosalts); and (3) gold–stibnite with quartz–stibnite association with fahlore, chalcostibite, and chalcopyrite.

The petrography and mineralogy of ore-bearing metasomatites are characterized in (Artemiev, 2016). The technological properties of refractory gold–sulphide ores are summarized in (Tolkanov et al., 2019).

The combination of different mineral and structural types of mineralization within the Mayskoe deposit determines the morphological diversity of ores and significantly complicates their genetic interpretation.

SAMPLES AND METHODS

Samples to study from the collection of B.S. Andreev (NEISRI FEB RAS) (Andreev, 1984) were taken from ore body 1. They are represented by silicified siltstones with disseminated pyrite-arsenopyrite mineralization.

The chemical composition of the studied sulphides was determined using a JXA-8200 electrone microprobe analyzer (JEOL) (EMPA method) in the Institute of Geology of Ore Deposits, Petrography, Mineralogy, and Geochemistry, Russian Academy of Sciences (IGEM RAS) (analyst E.V. Kovalchuk). In addition to macrocomponents (As, Fe, S) and major trace elements (Ni, Zn, Sb, Co, Cu, Ag) in pyrite and arsenopyrite, Au content (measurement detection limit (3σ) 45 ppm) was measured following the methodology described in detail in (Kovalchuk et al., 2019).

Trace elements in sulphides were determined by laser ablation-inductively coupled plasma-mass spectrometry (LA-ICP-MS) on an Agilent 7700x quadrupole mass spectrometer at the Institute of Mineralogy, Ural Branch, Russian Academy of Sciences (analyst D.A. Artemiev) and ThermoXSeries 2 quadrupole mass spectrometer equipped with a NewWaveResearch UP-213 laser ablation system at the laboratory of the IGEM RAS (analyst E.A. Minervina). The flux density was 1.8–5.5 J/cm^2 for pyrite and 3.0–4.5 J/cm^2 for arsenopyrite. Analyses were spot or linear, with a 30- to 55-μm laser beam. In total, 15 spot and 13 profile samples of pyrite and 12 spot and 11 profile samples of arsenopyrite were analyzed using laser sampling. The external calibration standard is USGS MASS-1 and UQAC FeS-1. The internal standard (IS) for pyrite and arsenopyrite is ^{57}Fe. The Fe content measured by the EMPA method was used for a quantitative analysis.

RESULTS OF ARSENOPYRITE STUDY

Arsenopyrite is represented by euhedral and subhedral crystals of an ~150-μm-long elongated-prismatic habit (elongation coefficient up to 1 : 10) forming specific stellate aggregates (Fig. 3).

As usual, arsenopyrite has a complex zonal structure visible under a polarizing microscope with crossed nicols (Figs. 4a, 4b). In addition to the thin oscillatory zonality, arsenopyrite crystals show a change in the crystal growth orientation, forming the clearly visible central (I) and outer (II) zones (Figs. 4c, 4d). Backscattered electron imaging of the surface of transverse rhomboid-shaped sections of arsenopyrite crystals confirmed this zoning pattern (Figs. 4–6) due to the variations in As and S contents. The As/S ratio in the central, darker (BSE image) zone I is 0.7–0.8. The As/S ratio in the lighter zone II, toward the rims of the crystals, increases to 1.17. The amount of Fe (at %) in zone I varies from 34.8 to 35.2, in the light outer zone II, it varies from 34.07 to 35.4. According to EMPA data, arsenopyrite in single analytical points contains Co (0.07–0.08 wt %), Ni (0.07–0.08 wt %), and Cu (0.09–0.15 wt %). Antimony (0.06–2.06 wt %) is a common impurity, and Sb distribution forms an oscillatory pattern with a tendency of increasing its content from the cores to the rims of the crystals (Fig. 5).

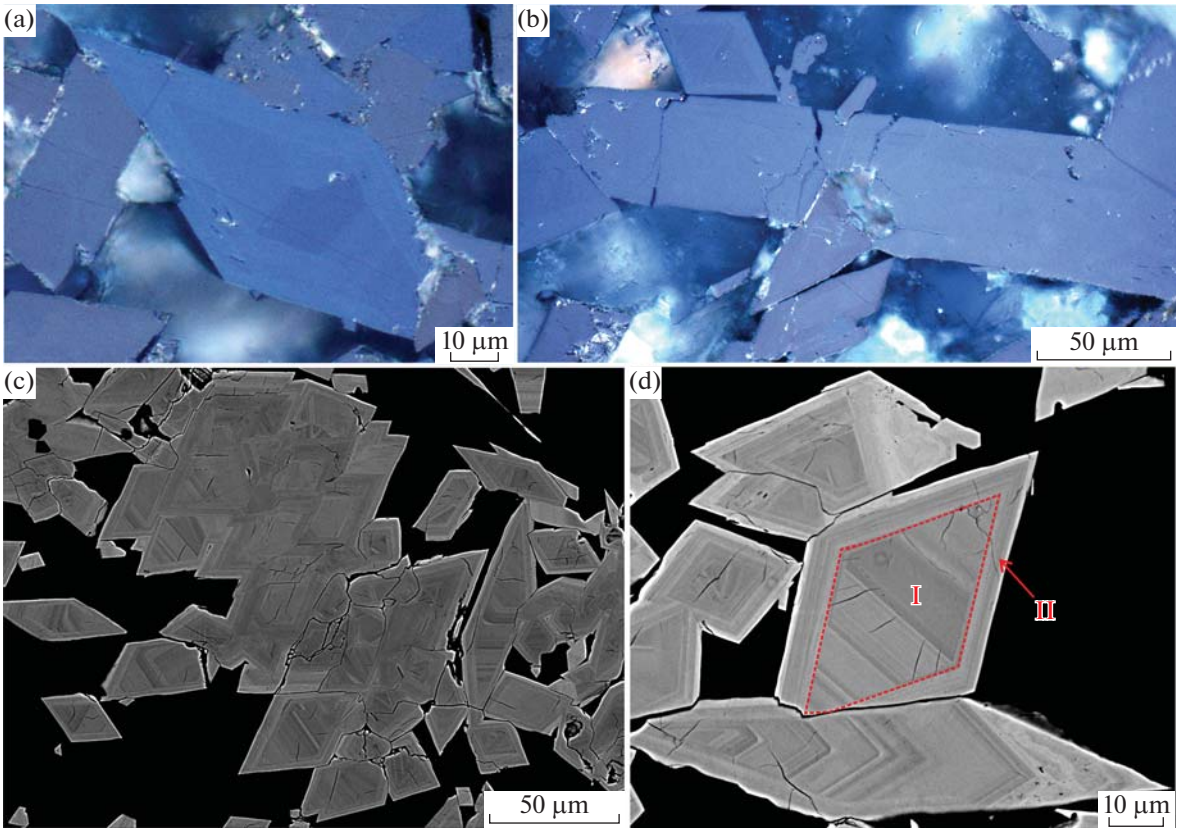

Fig. 4. Zonal arsenopyrite of the Mayskoe deposit: (a, b) reflected polarized light photomicrographs, crossed nicols; (c, d) BSE images, central zone I and outer zone II are shown in red.

According to EMPA data, the Au content in arsenopyrite is above the measurement detection limit in 75% of all analytical points and reaches 0.47 wt %. Based on probing profiles of longitudinal sections of individual crystals by main macrocomponents and gold, it was revealed that the darker (in backscattered electrons), i.e., more sulfurous, central parts of crystals are enriched in gold. Toward the rims, the gold content decreases by an order of magnitude in lighter (in backscattered electrons), respectively more As-rich zones (Figs. 5, 6). In this case, the Au distribution is extremely irregular even within the central zones of crystals and, as can be seen from the plots in Fig. 6, the maximum Au content is recorded in certain areas in zone I. The gold-distribution map (Fig. 7) over the cross-sectional area of an arsenopyrite crystal also shows that the maximum Au contents are characteristic of lighter (= more As-rich) thin zones within central zone I.

No significant correlation between gold and macrocomponents was observed for the entire sample of data (Fig. 8), although, at a gold content >0.1 wt %, the correlation coefficient for Au–As pair is 0.5 (at n = 24). Maximum gold contents (from 0.25 to 0.47 wt %) correspond to As/S ratios equal to 0.93–0.96. Au contents from 0.1 to 0.21 wt % correspond to the As/S ratio of 0.8–0.95. Au contents from 0.0045 to 0.1 wt % correspond to the As/S ratio of 0.7–0.92. In the probing profiles of single crystals, the inverse correlation of gold and antimony is traced (Fig. 5).

In the cross sections of arsenopyrite crystals there are distinct cracks that do not extend beyond the dark zone. This suggests that the outer arsenic zones overgrew with some interruption the earlier more sulfurous ones. In confirmation of this, Fig. 4d shows uneven porous light areas, which separate the outer and inner zones. This may indicate dissolution of a crystal during a pause or change in the conditions of crystallization.

In total, 35 analyses of arsenopyrite were performed by LA-ICP-MS. The contents of the most common trace elements (Co, Ni, Cu, Ag, Sb, Au, Tl, Pb, Bi) that are present in 70–90% of samples are given in Table 1. The following elements were found in 20–40% of all samples (maximum value, in ppm): Zn (40), Se (39), Sn (12), W (9), and Hg (30). Although the laser beam does not capture thin zones, some trace-element distribution patterns were nevertheless identified based on the laser profiling data. The central, more sulfurous zones of arsenopyrite contain higher Au and Pb contents. Co and Ni contents are below the measurement detection limit. Also, a lower

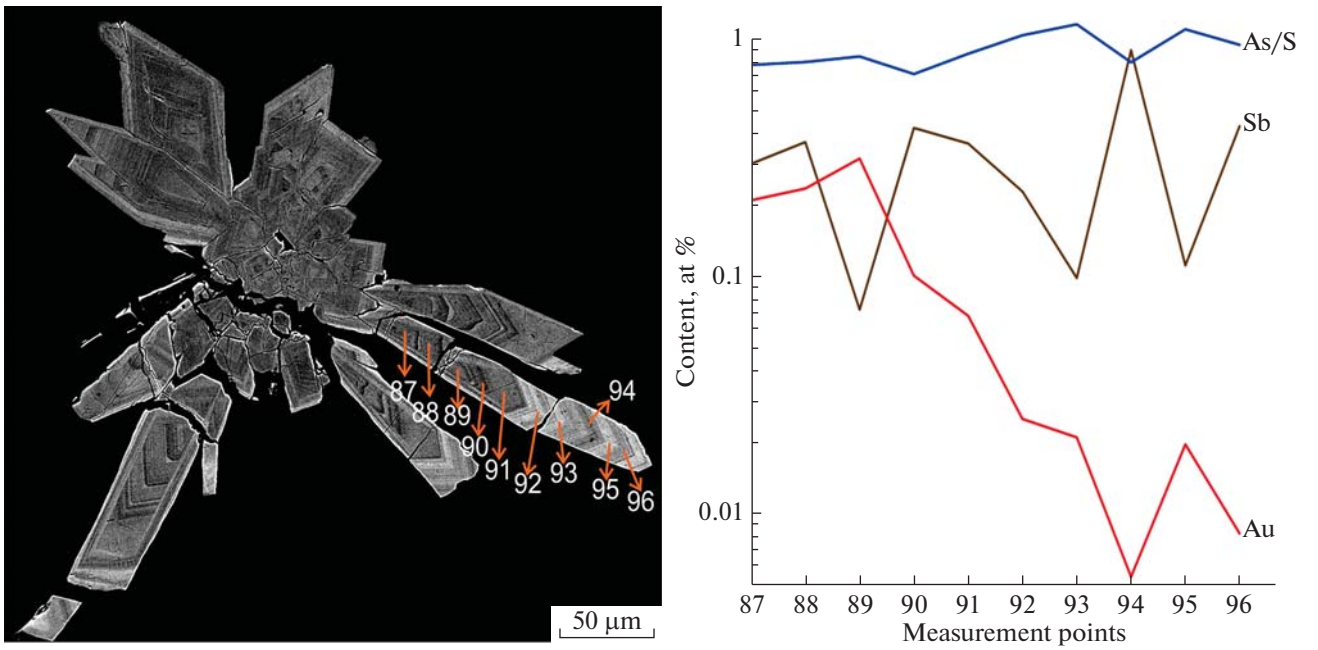

Fig. 5. Distribution of Au, Sb, As, and S (As/S ratio) in arsenopyrite crystal (BSE image), according to EMPA data. Figures in the photo correspond to the analysis points on the plot.

content of Cu (50–60 ppm) in the central dark (BSE) parts of the grains there is common. Co and Ni are concentrated in the outer As-rich zones, and Sb content increases. Cu and Bi show relatively uniform distribution, however, their increased contents are also confined to rims of grains. When the profile crosses cracks and porous zones in arsenopyrite, or when the arsenopyrite-hosted medium is trapped, the group of elements Tl–Co–Ni–Pb–Cu ± Bi ± Ag ± W form joint bursts of signals in the ablation spectra. A significant positive correlation in arsenopyrite was established for Ni–Co ($r = 0.95$), Co–Bi ($r = 0.71$), Ni–Bi ($r = 0.77$), Cu–Ag ($r = 0.84$), Cu–Tl ($r = 0.7$), and Ag–Tl ($r = 0.76$) pairs under $n = 35$.

RESULTS OF PYRITE STUDY

Anhedral pyrite aggregates have a zonal structure with porous central and smooth outer zones with crystallographic habit. As seen in BSE images, pyrite grains have heterogeneous composition with varying As content. According to the composition and structural features, there are four zones in pyrite (Fig. 9): (1) central porous zone, As content does not exceed 0.5 wt %; (2) thin As-rich halos (2–30 μm) overgrowing porous zones (up to 5.3 wt % As); (3) thinly zonal outer zone with crystallographic outlines and As content up to 1.8 wt %; (4) outer porous zone of irregular thickness (0–20 μm), with less than 0.06 wt % As. There are the following impurities in pyrite (according to EMPA

Table 1. Contents of trace elements in arsenopyrite and pyrite from the Mayskoe deposit according to LA-ICP-MS data.

Mineral	C, ppm	Co	Ni	Cu	Ag	Sb	Au	Tl	Pb	Bi
Arsenopyrite ($n = 35$)	min	0.4	8.6	50	0.7	978	52	0.01	2.3	1.7
	max	70	370	892	117	10702	922	42	270	32.3
	GM	11	84	202	3.7	4409	340	1.7	37	8.0
	fr. occ., %	79	85	97	74	100	100	91	100	91
Pyrite ($n = 46$)	min	0.3	4	47	0.1	1	0.3	0.01	0.7	0.2
	max	83	307	693	6.1	321	55	13	716	18
	GM	10.5	46	169	1	40	8	0.2	25	1.5
	fr. occ., %	100	98	100	78	100	100	80	100	70

Element contents are given in ppm; GM—geometric mean, defined as the root of the nth degree from the product of n numbers; fr. occ.—frequency of occurrence of a component.

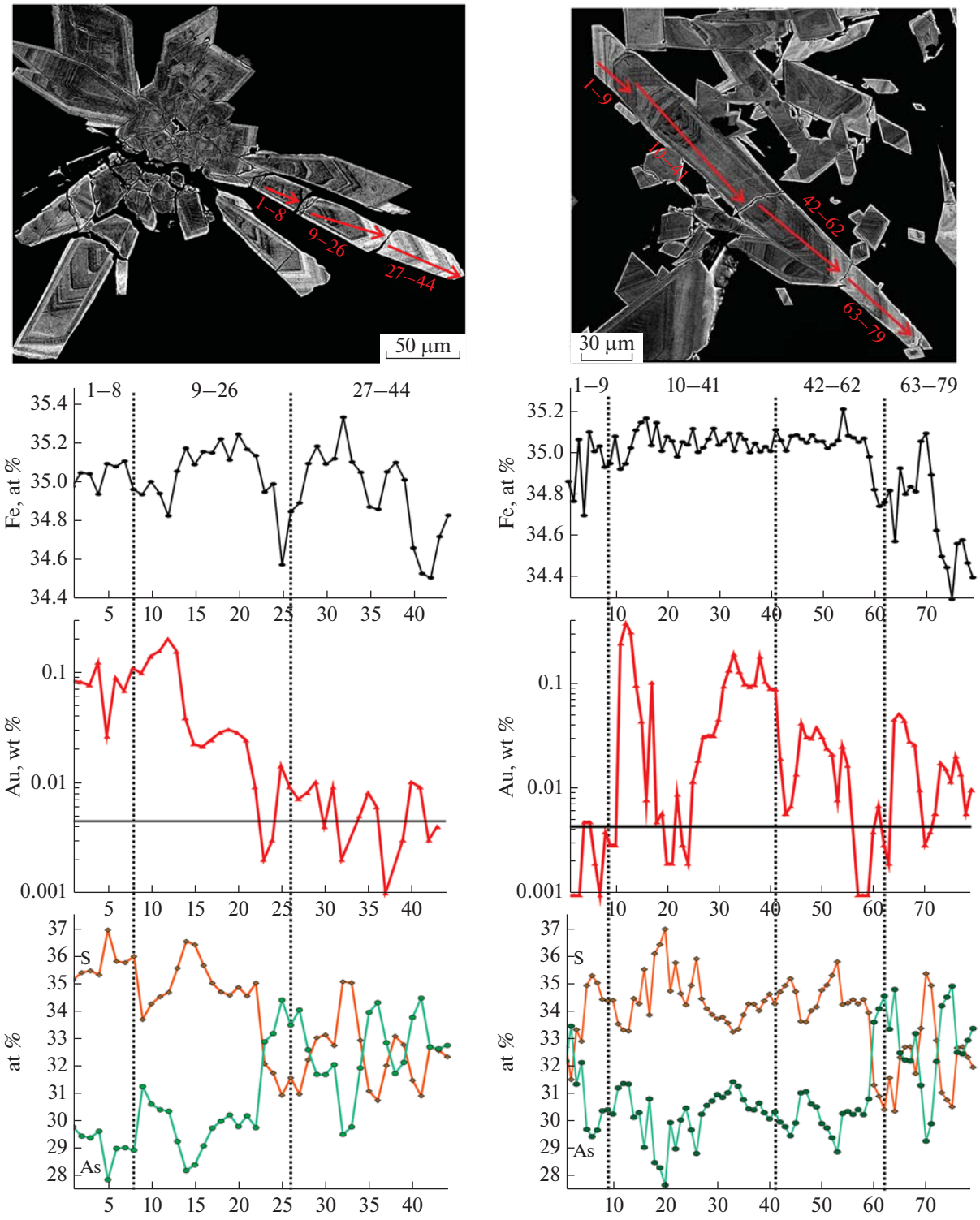

Fig. 6. Probing profiles in arsenopyrite crystals with Fe, S, and As (at %) and Au (wt %) distribution plots. Numbers on BSE-images correspond with points on probing-profile.

data): Cu up to 0.11 wt %, in single points; Co up to 0.08 wt %, in 30% of analyses; Au content exceeding the measurement detection limit (0.0045 wt %) in a half of analytical points and reaches 0.012 wt %. Figure 10 shows the variation in Au content along the electron probing profile of pyrite grains. The maximum Au contents are confined to light-colored zones with increased As content. However, no significant correla-

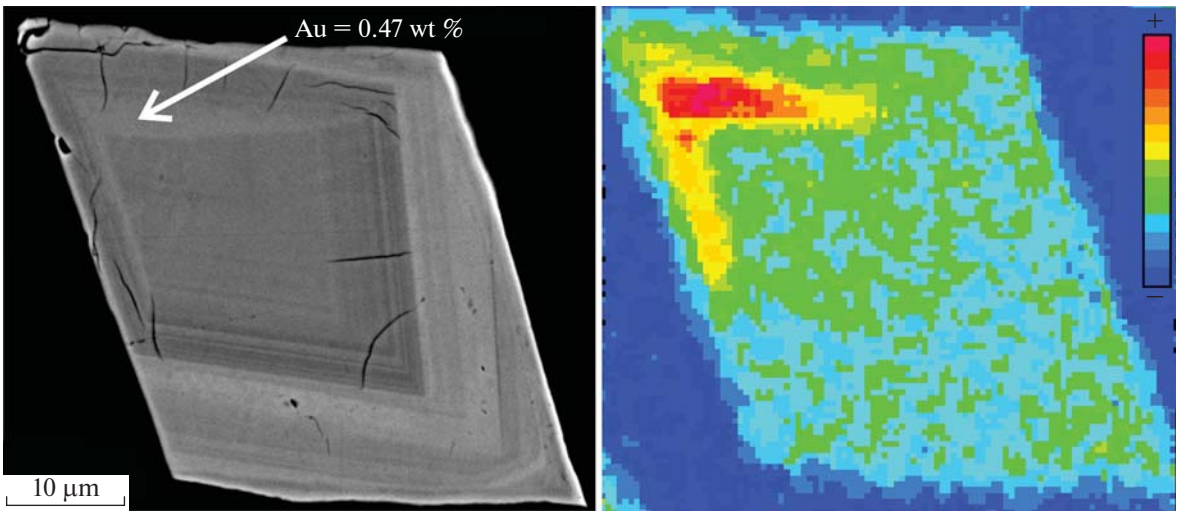

Fig. 7. Zonal arsenopyrite metacrystal. (a) BSE image; (b) Au distribution map based on EMPA data: Au (Mα, PETH), current 20 nA, time 100 ms.

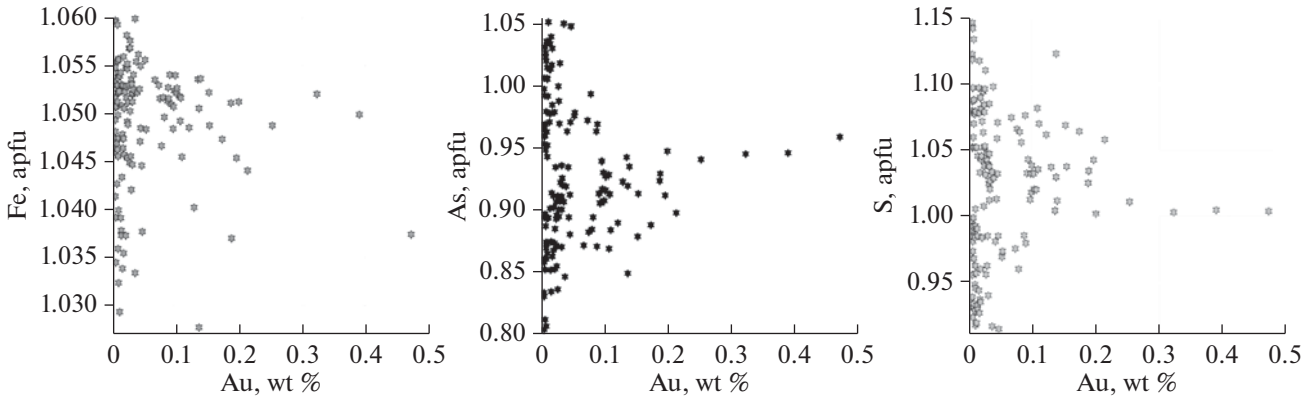

Fig. 8. Diagrams of macrocomponent contents (in formula units) and gold content (wt %) in arsenopyrite, based on EMPA data.

tion between As and Au for the whole sample was found.

The LA-ICP-MS method was used to perform 46 pyrite analyses. The content range and mean values of the most widespread trace elements (Co, Ni, Cu, Ag, Sb, Au, Tl, Pb, Bi) are given in the table. The following elements (max, in ppm) were detected in 20–50% of the samples: Zn (13), Se (15), Sn (4), W (23), and Hg (6). In single samples, pyrite contains Ga, Ge, In, and Te in minor amounts. Based on LA-ICP-MS data, the central, porous parts of pyrite aggregates contain higher contents of the following elements (ppm): Pb (17–716, GM = 117); Sb (45–320, GM = 121); Bi (0.4–18, GM = 3.2); Tl (up to 0.8); Ag (0.4–6, GM = 2); Zn (up to 13); and partially Co (10–83, GM = 30); and Ni (21–237, GM = 75); (Figs. 10, 11). There also occur V, Ga, Ge, Te, and W. There are lower As and Au contents (0.3–4 ppm) (Fig. 11). The Au content increases to the edges of grains, up to 30 ppm on average. The Co, Ni, Ag, Tl, and Bi contents decrease towards the edges up to the measurement detection limit. The contents of Pb (0.7 ppm) and Sb (1.13 ppm) decrease reaching the minimum values. Based on high correlation coefficients in the groups Pb–Bi–Sb (r = 0.9) and Ag–Bi and Ag–Pb (r = 0.7), at n = 46, it can be assumed that these elements input in the pyrite composition in the form of galena microinclusions or bismuth and antimony sulfosalts. A significant correlation is noted for Co–Ni (r = 0.7) and Au–As (r = 0.8) pairs (Fig. 12). Copper is the only impurity trace element whose distribution in the ablation spectra of pyrite is relatively uniform.

DISCUSSION

Gold-bearing arsenopyrite from disseminated ores of the Mayskoe deposit usually has a zonal structure with a more sulfurous (As/S = 0.7–0.8) central zone I and more arsenic (As/S up to 1.17) outer zone II (Fig. 4).

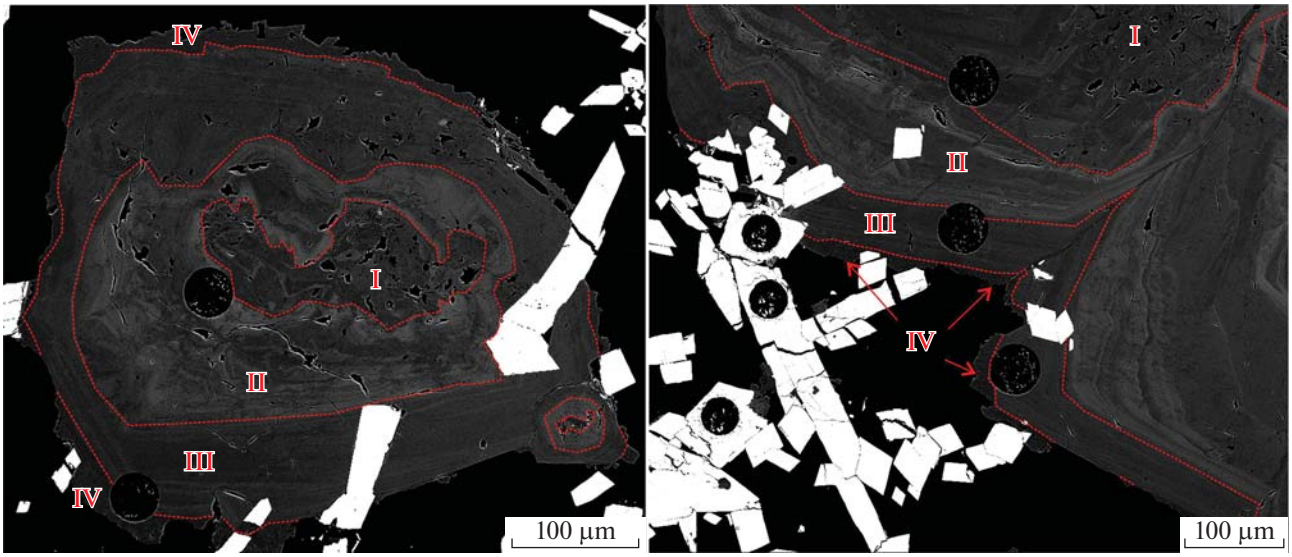

Fig. 9. BSE images of intergrowths of pyrite metacrystals (dark) with arsenopyrite (light); dotted lines separate zones in pyrite indicated by Roman numerals (see text).

At the same time, its composition changes discontinuously and a change in the crystallographic orientation of crystal growth is observed. A similar complex pattern of zonation was described in gold-bearing arsenopyrite from the Villeranges deposit (Benzaazoua et al., 2007). Here, however, the more arsenic outer zones are highly enriched in gold. In the arsenopyrite of the Mayskoe deposit, the maximum Au content (up to 0.47 wt %) is recorded in thin (5–10 μm) more arsenic areas within the central zone I (Figs. 6, 7). In the more arsenic zones, the Au content is an order of magnitude lower (Figs. 5, 6).

Arsenopyrite from disseminated ores of the Mayskoe deposit demonstrates inverse Au–Fe and Au–Sb correlation and direct Au–As correlation.

The correlation of gold with macrocomponents is discussed for both natural and synthetic arsenopyrite crystals (Fleet and Mumin; 1997; Genkin et al., 1998; Cabri et al., 2000; Vykentiev, 2015; Kovalchuk et al., 2019). Thus, direct Au–As correlation and inverse Au–Fe correlation in arsenopyrite are noted in a number of deposits, e.g., Vorontsovskoe (Kovalchuk et al., 2019; Vikentyev et al., 2019; Tyukova et al., 2022), Villeranges and Le Chatelet (France) (Cathelineau et al, 1989; Marcoux et al., 1989), etc. Antagonistic distribution of Sb and Au in gold-bearing arsenopyrite is indicated in many deposits (Marcoux et al., 1989; Genkin, 1998; Genkin et al., 1998; Li et al., 2019; Ashley et al., 2000; Sidorova et al., 2022; etc.).

Pyrite from the disseminated gold–sulphide ores of the Mayskoe deposit also has a zonal structure with clearly visible four zones (Figs. 9–11): (1) central porous, with lower As and Au contents and a higher Pb–Sb–Co–Ni–Bi–Tl–Ag content; (2) thin, As-rich (up to 5.3 wt %) and Au-rich (up to 0.012 wt %) halos; (3) an outer thin zone, depleted in other elements, with As up to 1.8 wt % and Au up to 30 ppm with decreasing its content towards the grain edge to 6 ppm; and (4) an outer porous zone, up to 20 μm thick, containing less than 0.06 wt % As.

The classical case of "invisible" gold accumulation in thin arsenic rims in pyrite is also known for the Karlin-type deposits. Here, early pre-ore pyrite is overgrown by ore pyrite enriched with trace elements, including arsenic and gold (Palenik et al., 2004; Large et al., 2009; Muntean et al., 2011; Gopon et al., 2019; Large and Maslennikov, 2020; Liang et al., 2021). Gold-bearing pyrite of the Mayskoe deposit differs from "Karlin-type" pyrite in that the outer zones enriched in gold and arsenic are depleted in other elements.

Relationships of Coexisting Gold-Bearing Sulphides at the Mayskoe and Other Deposits with "Invisible" Gold

According to experimental data (Clark, 1966), the pyrite–arsenopyrite paragenesis is stable in the temperature range of about 200–491°C. Using the example of a number of deposits in northeastern Russia, it was established that associations with arsenopyrite are formed at the temperature of not below 250 ± 50°C (Tyukova and Voroshin, 2007). Based on our data, one can assume that zone I in pyrite was formed before the inflow of As- and Au-rich solutions into the ore-forming system, while thin zones II of high-Au arsenic pyrite of the Mayskoe deposit grew under conditions of rapid crystallization with increasing temperature and increasing As and Au contents. Arsenopyrite began to crystallize at the end of growth of zone II; the further growth occurred simultaneously with the zone

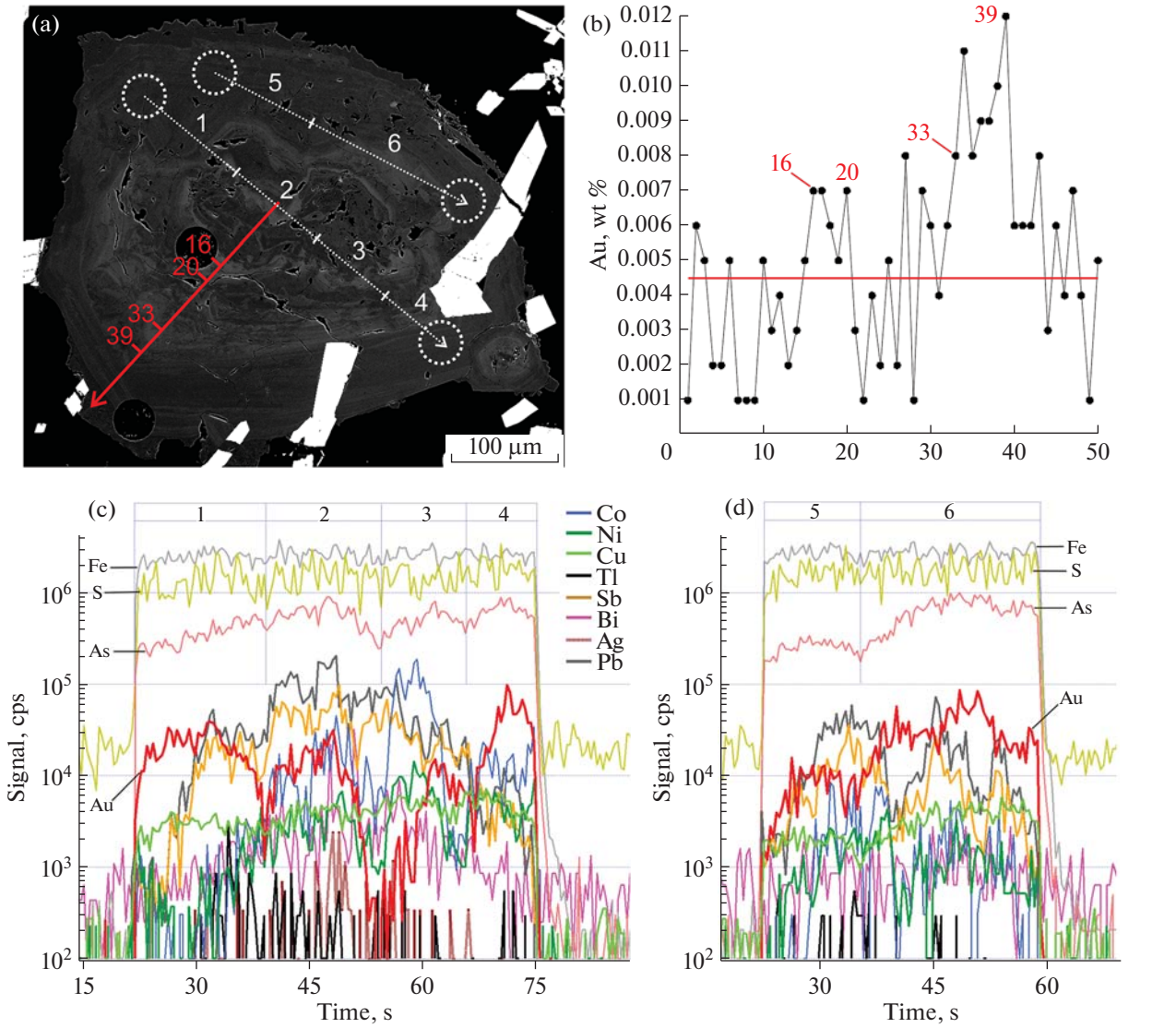

Fig. 10. (a) BSE image of the intergrowth of metacrystal pyrite (dark) with arsenopyrite (light); red arrow indicates the 5-μm electron probing profile shown in Fig. 10b; white dashed arrows indicate the position of laser ablation profiles at intervals (1–6) shown in Figs. 10c and 10d.

III of pyrite. The outer porous zones IV of pyrite, which are significantly depleted in Au and As, were probably formed at the post-ore stages.

When a certain temperature is reached, sulfuric arsenopyrite with the highest Au content begins to grow, while the gold in pyrite zone III decreases. As has been established for many deposits and confirmed empirically (Mumin et al., 1994; Fleet and Mumin, 1997; Morey et al., 2008; Sung et al., 2009; Cook et al., 2013), under equilibrium crystallization of coexisting pyrite and arsenopyrite, arsenopyrite will be characterized by a higher gold content. Further, an abrupt change in crystallization conditions is traced, as evidenced by indistinct growth zones in pyrite (Figs. 9–11) and arsenopyrite (Fig. 4d), a change in the composition and orientation of growth of arsenopyrite, as well as cracks in the central sulfur zones (Fig. 7). Some enrichment in As in the outer zones of arsenopyrite and, on the contrary, depletion in As in the outer zones and partial dissolution of pyrite may be due to the increase in alkalinity of solutions (Kolonin et al., 1988).

The following data on the composition and distribution of trace elements were previously obtained for the Olympiada and Kyuchus deposits of similar gold–sulphide–antimony industrial type with “invisible” gold in sulphides. According to the data of (Genkin et al., 1994, 1998), the highest Au contents in the sulphides of the Olympiada deposit correspond to the As- and Sb-depleted areas. Mössbauer spectroscopy revealed both chemically bound and metallic forms of gold in arsenopyrite. In (Sazonov et al., 2019; Sily-

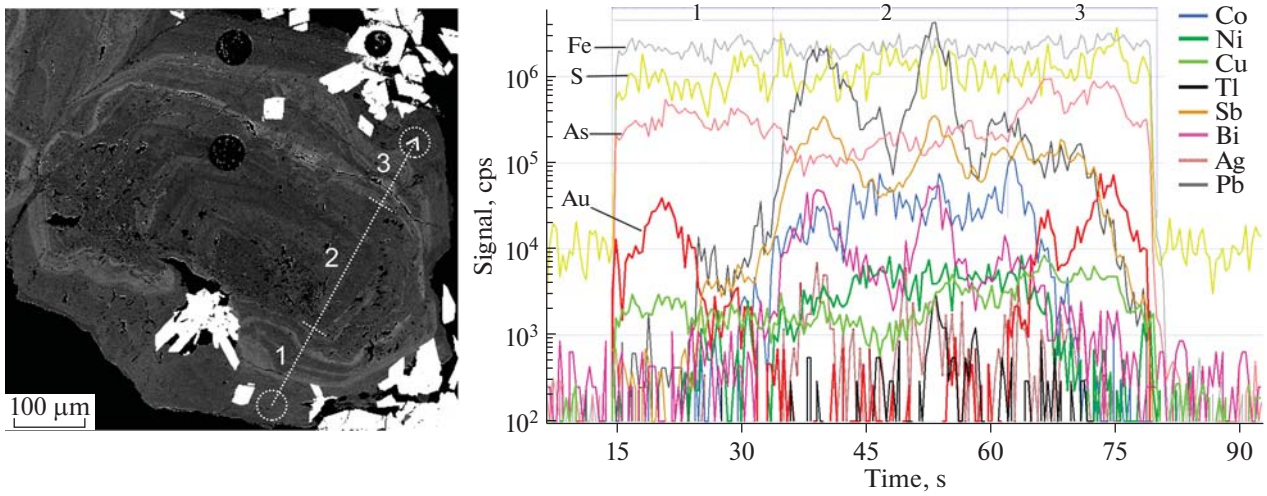

Fig. 11. On the left: BSE image of an intergrowth of pyrite metacrystal (dark) with arsenopyrite (light); on the right: the laser ablation profile at intervals (1–3) is indicated by a white dashed arrow.

anov, 2020; Silyanov et al., 2021), it was established that arsenopyrite of the Olympiada deposit has a direct Au–Fe correlation and an inverse Au–Sb and S/As–Sb correlation. In addition, pyrite from the Olympiada deposit is characterized by low As and Au contents.

The enrichment of the marginal parts of crystals of both minerals in Au and As was established in zonal arsenopyrite and pyrite of the Kyuchus deposit, but no significant correlation between Au with other elements in the whole sample was identified (Sidorova et al., 2022). It was noted that gold was concentrated partially in sulphides during their growth, mainly in acicular arsenopyrite. Another part of gold occurs in fragments of carbonaceous–silicate matrix in cell and sieve zones of pyrite and arsenopyrite together with a group of elements (As–Sb–Tl–Hg–Pb–Bi–Ag–Cu–Zn, etc.).

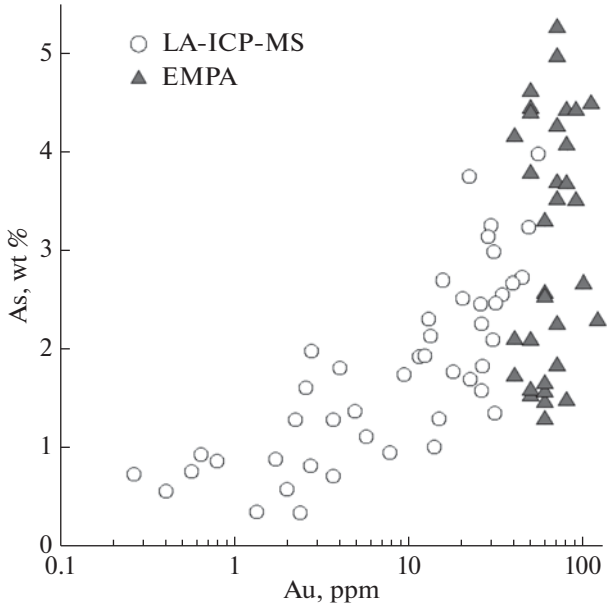

Fig. 12. Diagram of Au (in ppm) and As (wt %) contents in pyrite of the Mayskoe deposit, based on EMPA and LA-ICP-MS data.

CONCLUSIONS

The regularities of behavior of trace elements and "invisible" gold in gold-bearing sulphides from disseminated ores of the Mayskoe deposit (Central Chukotka) were established using modern precision methods. Based on the data obtained, the sequence of crystallization and relationships of gold-bearing sulphides at the main and most productive gold–sulphide stage of the deposit formation were established.

Arsenopyrite from disseminated ores has a zonal structure with more sulfurous central zone and more arsenic outer zone, with maximum gold content (up to 0.47 wt %) in thin (5–10 μm) arsenic areas in the central, more sulfurous, zones of crystals. The Au–Fe and Au–Sb inverse correlation and Au–As direct correlation were established for arsenopyrite.

Pyrite is characterized by a complex zonal structure of xenomorphic aggregates with central "relict" zones (with increased contents of trace elements (Pb, Sb, Co, Ni, Bi, Tl, Ag, Zn, and low contents of As and Au) and subsequent overgrow with more arsenic gold-bearing pyrite (zones II, III). Zone II is characterized by the development of thin aureoles with maximum As (up to 5.3 wt %) and Au (up to 0. 012 wt %) contents. The later zone, zone III, is in equilibrium with gold-bearing arsenopyrite. Due to this, Au is mostly concentrated in the latter, and the Au content in zone-III in pyrite does not exceed 30 ppm with uniform distribution of Au and As.

ACKNOWLEDGMENTS

We would like to thank the reviewers and the editors of *Geology of Ore Deposits* for their thorough reading and comments, which helped us to significantly improve this paper.

FUNDING

This work was performed within the framework of a state assignment of Institute of Geology of Ore Deposits, Petrography, Mineralogy, and Geochemistry of Russian Academy of Sciences, project no. 124022400144–6.

CONFLICT OF INTEREST

The authors of this work declare that they have no conflicts of interest.

REFERENCES

Andreev, B.S., Mineralogical and geochemical features and conditions of formation of rare-metal-antimony occurrence, *Extended Abstract of Candidate's (Geol.-Min.) Dissertation*, Leningrad, 1984, p. 224.

Artem'ev, D.S., Petrography and mineralogy of ore-bearing hydrothermal-metasomatic formations of the Maiskoe gold deposit (Central Chukotka), *Regional. Geol. Metallogen.*, 2016, vol. 67, pp. 118–123.

Ashley, P.M., Creagh, C.J., and Ryan, C.G., Invisible gold in ore and mineral concentrates from the Hillgrove gold-antimony deposits, NSW, Australia, *Miner. Deposita*, 2000, vol. 35, no. 4, pp. 285–301.
https://doi.org/10.1007/s001260050242

Benzaazoua, M., Marion, P., Robaut, F., and Pinto, A., Gold-bearing arsenopyrite and pyrite in refractory ores: analytical refinements and new understanding of gold mineralogy, *Mineral. Mag.*, 2007, vol. 71, no. 2, pp. 123–142.
https://doi.org/10.1180/minmag.2007.071.2.123

Bortnikov, N.S., Bryzgalov, I.A., Krivitskaya, N.N., Prokof'ev, V.Yu., and Vikent'eva, O.V., The Maiskoe multimegastage disseminated gold–sulfide deposit (Chukotka, Russia): mineralogy, fluid inclusions, stable isotopes (O and S), history, and conditions of formation, *Geol. Ore Deposits*, 2004, vol. 46, no. 6, pp. 409–440.

Cabri, L.J., Newville, M., Gordon, R.A., Crozier, E.D., Sutton, S.R., Mcmahon, G., and Jiang, D.-T., Chemical speciation of gold in arsenopyrite, *Can. Mineral.*, 2000, vol. 38, no. 5, pp. 1265–1281.
https://doi.org/10.2113/gscanmin.38.5.1265

Cook, N.J., Ciobanu, C.L., Meria, D., Silcock, D., and Wade, B., Arsenopyrite-pyrite association in an orogenic gold ore: tracing mineralization history from textures and trace elements, *Econ. Geol.*, 2013, vol. 108, no. 6, pp. 1273–1283.
https://doi.org/10.2113/econgeo.108.6.1273

Fleet, M.E. and Mumin, A.H., Gold-bearing arsenian pyrite and marcasite and arsenopyrite from Carlin Trend gold deposits and laboratory synthesis, *Am. Mineral.*, 1997, vol. 82, nos. 1–2, pp. 182–193.
https://doi.org/10.2138/am-1997-1-220

Gavrilov, A.M., Pleshakov, A.P., Bernshtein, P.S., and Sandomirskaya, S.M., Submicroscopic gold in sulfides of some disseminated ore deposits, *Sov. geologiya*, 1982, no. 8, pp. 81–86.

Gavrilov, A.M., Novozhilov, Yu.I., and Sidorov, A.A., On affiliation of gold-arsenic-antimony mineralization to the "disseminated sulfide ores with finely dispersed gold," *Tikhookean. Geol.*, 1986, no. 3, pp. 108–111.

Genkin, A.D., Gold-bearing arsenopyrite from gold deposits: Internal structure of grains, composition, mechanism of growth, and gold state, *Geol. Ore Deposits*, 1998, vol. 40, no. 6, pp. 490–496.

Genkin, A.D., Bortnikov, N.S., Cabri, L.J., Wagner, F.E., Stanley, Ch.J., Safonov, Yu.G., McMahon, G., Friedl, J., Kerzin, A.L., and Gamyanin, G.N., A multidisciplinary study of invisible gold in arsenopyrite from four mesothermal gold deposits in Siberia, Russian Federation, *Econ. Geol.*, 1998, vol. 93, no. 4, pp. 463–487.
https://doi.org/10.2113/gsecongeo.93.4.463

Genkin, A.D., Lopatin, V.A., Savel'ev, R.A., Safonov, Yu.G., Sergeev, N.B., Kerzin, A.L., Tsepin, A.I., Amshtutts, Kh., Afanas'eva, Z.B., Vagner, F., and Ivanova, G.F., Gold ores of the Olympiada deposit (Yeniseisky Ridge, Siberia), *Geol. Rud. Mestorozhd.*, 1994, vol. 36, no. 2, pp. 111–136.

Gopon, P., Douglas, J.O., Auger, M.A., Hansen, L., Wade, J., Cline, J.S., Robb, L.J., and Moody, M.P., A Nanoscale investigation of Carlin-Type gold deposits: An atom-scale elemental and isotopic perspective, *Econ. Geol.*, 2019, vol. 114, no. 6, pp. 1123–1133.
https://doi.org/10.5382/econgeo.4676

Grigorov, S.A., Samorukov, N.M., Samorukova, L.N., and Tomilov, V.L., *Report of the Tamnekvun Geological Survey Party on a Scale 1 : 50000 for 1971–1972*, Pevek, 1973, vol. 1.

Klark, L., Phase relations in the Fe–As–S system, *Problemy endogennykh mestorozhdenii*, 1966, no. 3, pp. 160–250.

Kolonin, G.R., Pal'yanova, G.A., and Shironosova, G.P., Stability and solubility of arsenopyrite in hydrothermal solutions, *Geokhimiya*, 1988, no. 6, pp. 843–855.

Kovalchuk, E.V., Tagirov, B.R., Vikentyev, I.V., Chareev, D.A., Tyukova, E.E., Nikol'skii, M.S., Borisovskii, S.E., and Bortnikov, N.S., "Invisible" gold in synthetic and natural arsenopyrite crystals, Vorontsovka Deposit, Northern Ural, *Geol. Ore Deposits*, 2019, vol. 61, no. 5, pp. 447–468.

Kovalev, K.R., Kuz'mina, O.N., Vladimirov, B.A., Kalinin, A.G., Naumov, Yu.A., Kirillov, E.A., Annikova, M.V., and Yu, I., Disseminated gold–sulfide mineralization at the Zhaima Deposit, Eastern Kazakhstan, *Geol. Ore Deposits*, 2016, vol. 58, no. 2, pp. 116–133.

Large, R.R., Danyushevsky, L., Hollit, C., Maslennikov, V., Meffre, S., Gilbert, S., Bull, S., Scott, R., Emsbo, P., Thomas, H., Singh, B., and Foster, J., Gold and trace element zonation in pyrite using a laser imaging technique: Implications for the timing of gold in orogenic and Carlin-style sediment-hosted deposits, *Econ. Geol.*, 2009, vol. 104, no. 5, pp. 635–668.
https://doi.org/10.2113/gsecongeo.104.5.635

Large, R.R. and Maslennikov, V.V., Invisible Gold Paragenesis and geochemistry in pyrite from orogenic and sediment-hosted gold deposits, *Minerals*, 2020, vol. 10, no. 4, p. 339.
https://doi.org/10.3390/min10040339

Li, W., Cook, N.J., Xie, G.-Q., Mao, J.-W., Ciobanu, C.L., Li, J.-W., and Zhang, Z.-Y., Textures and trace element signatures of pyrite and arsenopyrite from the Gutaishan Au–

Sb deposit, South China, *Mineral. Deposita*, 2019, vol. 54, no. 4, pp. 591–610.
https://doi.org/10.1007/s00126-018-0826-0

Liang, Q.-L., Xie, Zh., Song, X.-Y., Wirth, R., Xia, Yo., and Cline, J., Evolution of invisible Au in arsenian pyrite in Carlin-type Au deposits, *Econ. Geol.*, 2021, vol. 116, no. 2, pp. 515–526.
https://doi.org/10.5382/econgeo.4781

Marcoux, É., Bonnemaison, M., Braux, C., and Johan, Z., Distribution de Au, Sb, As et Fe dans l'arsénopyrite aurifère du Çhâtelet et de Villeranges (Greuse, Massif Central français, *Comptes Rendus de l'Académie des Sciences,* 1989, vol. 308, pp. 293–300.

Morey, A.A., Tomkins, A.G., Bierlein, F.P., Weinberg, R.F., and Davidson, G.J., Bimodal distribution of gold in pyrite and arsenopyrite: Examples from the Archean Boorara and Bardoc shear systems, Yilgarn Craton, Western Australia, *Econ. Geol.*, 2008, vol. 103, no. 3, pp. 599–614.
https://doi.org/10.2113/gsecongeo.103.3.599

Mumin, A.H., Fleet, M.E., and Chryssoulis, S.L., Gold mineralization in As-rich mesothermal gold ores of the Bogosu-Prestea mining district of the Ashanti Gold Belt, Ghana: remobilization of "invisible" gold, *Mineral. Deposita*, 1994, vol. 29, no. 6, pp. 445–460.
https://doi.org/10.1007/bf00193506

Muntean, J.L., Cline, J.S., Simon, A.C., and Longo, A.A., Magmatic–hydrothermal origin of Nevada's Carlin-type gold deposits, *Nat. Geosci.*, 2011, vol. 4, no. 2, pp. 122–127.
https://doi.org/10.1038/ngeo1064

Novozhilov, Yu.I. and Gavrilov, A.M., *Zoloto-sul'fidnye mestorozhdeniya v terrigennykh uglerodistykh tolshchakh* (Gold-Sulfide Deposits in Terrigenous Carbonaceous Sequences), Moscow: TsNIGRI, 1999.

Novozhilov, Yu.N., Gavrilov, A.M., Sidorov, A.A., and Dr., *Izuchenie strukturnykh uslovii lokalizatsii i mineralogo-geokhimicheskikh osobennostei orudeneniya na Maiskom zolotorudnom mestorozhdenii* (Study of Structural Conditions of Localization and Mineralogical and Geochemical Peculiarities of Mineralization at the Maiskoe Gold Deposit), Moscow: TsNIGRI, 1983.

Novozhilov, Yu.I., Sidorov, A.A., Gavrilov, A.M., Volkov, A.V., Grigorov, S.A., and Protskii, A.G., Maiskoe deposit, *Zolotorudnye mestorozhdeniya SSSR. Tom IV. Geologiya zolotorudnykh mestorozhdenii Vostoka* (Gold Deposits of the USSR. Vol. IV. Geology of Gold Ore Deposits of the East USSR), Moscow: TsNIGRI, 1988, pp. 167–188.

Palenik, Ch.S., Utsunomiya, S., Reich, M., Kesler, S.E., Wang, L., and Ewing, R.C., "Invisible" gold revealed: Direct imaging of gold nanoparticles in a Carlin-type deposit, *Am. Mineral.*, 2004, vol. 89, no. 10, pp. 1359–1366.
https://doi.org/10.2138/am-2004-1002

Sazonov, A.M., Silyanov, S.A., Bayukov, O.A., Knyazev, Yu.V., Zvyagina, Ye.A., and Tishin, P.A., Composition and ligand microstructure of arsenopyrite from gold ore deposits of the Yenisei Ridge (Eastern Siberia, Russia), *Minerals*, 2019, vol. 9, no. 12, p. 737.
https://doi.org/10.3390/min9120737

Shilo, N.A., Sakharova, M.S., Krivitskaya, N.N., Ryakhovskaya, S.K., and Bryzgalov, I.A., *Mineralogicheskie i geneticheskie osobennosti zoloto-serebryanogo orudeneniya severo-zapadnoi chasti Tikhookeanskogo obramleniya* (Mineralogical and Genetic Features of Gold-Silver Mineralization of the Northwestern Pacific Margin), Moscow: Nauka, 1992.

Sidorova, N.V., Volkov, A.V., Koval'chuk, E.V., Minervina, E.A., and Levitskaya, L.A., Invisible gold and other impurity elements in pyrite and arsenopyrite of disseminated ores of the Kyuchus Deposit (Sakha Republic (Yakutia)), *Geol. Ore Deposits*, 2022, vol. 64, no. 5, pp. 281–291.

Silyanov, S.A., Geology and Mineralogical and Geochemical Indicators of Genesis of the Olympiada Gold Deposit (Yenisei Range), *Extended Abstract of Candidate's (Geol.-Min.) Dissertation*, Krasnoyarsk, 2020, p. 185.

Silyanov, S.A., Sazonov, A.M., Tishin, P.A., Lobastov, B.M., Nekrasova, N.A., Zvyagina, E.A., and Ryabukha, M.A., Trace elements in sulfides and gold of the Olimpiada Deposit (Yenisei Ridge): Ore substance sources and fluid parameters, *Russ. Geol. Geophys.*, 2021, no. 3, pp. 306–323.

Sung, Y.-H., Brugger, J., Ciobanu, C.L., Pring, A., Skinner, W., and Nugus, M., Invisible gold in arsenian pyrite and arsenopyrite from a multistage Archaean gold deposit: Sunrise Dam, Eastern Goldfields Province, Western Australia, *Miner. Deposita*, 2009, vol. 44, no. 7, pp. 765–791.
https://doi.org/10.1007/s00126-009-0244-4

Tolkanov, O.A., Heterogeneity of the material composition of gold-sulfide ores of the Maiskoye deposit, Northeast Russia, *Mineralogiya*, 2019, vol. 5, no. 2, pp. 69–82.

Tyukova, E.E., Vikentyev, I.V., Kovalchuk, E.V., Borisovsky, S.E., and Tagirov, B.R., Gold-bearing arsenian pyrite and arsenopyrite from Vorontsovka Carlinstyle gold deposit in the North Urals, *German International Journal of Modern Science*, 2022, no. 25, pp. 4–9.

Tyukova, E.E. and Voroshin, S.V., *Sostav i paragenezisy arsenopirita v mestorozhdeniyakh i vmeshchayushchikh porodakh Verkhne-Kolymskogo regiona (k interpretatsii genezisa sul'fidnykh assotsiatsii)* (Composition and Paragenesis of Arsenopyrite in Deposits and Host Rocks of the Upper Kolyma Region (to Interpretation of the Genesis of Sulfide Associations)), Magadan: SVKNII DVO RAN, 2007.

Vikentyev, I.V., Invisible and microscopic gold in pyrite: methods and new data for massive sulfide ores of the Urals, *Geol. Ore Deposits*, 2015, vol. 57, no. 4, pp. 237–266.

Vikentyev, I.V., Tyukova, E.E., Vikent'eva, O.V., Chugaev, A.V., Dubinina, E.O., Prokofiev, V.Yu., and Murzin, V.V., Vorontsovka Carlin-style gold deposit in the North Urals: Mineralogy, fluid inclusion and isotope data for genetic model, *Chem. Geol.*, 2019, vol. 508, pp. 144–166.
https://doi.org/10.1016/j.chemgeo.2018.07.020

Volkov, A.V., Goncharov, V.I., and Sidorov, A.A., *Mestorozhdeniya zolota i serebra Chukotki* (Gold and Silver Deposits of Chukotka), Magadan: SVKNII DVO RAN, 2006.

Volkov, A.V., Genkin, A.D., and Goncharov, V.I., Gold speciation in the ores of the Natalka and Maiskoye deposits (North-East Russia), *Tikhookean. Geol.*, 2007, vol. 25, no. 6, pp. 18–29.

Volkov, A.V. and Sidorov, A.A., Invisible gold, *Vestn. Ross. Akad. Nauk*, 2017, vol. 87, no. 1, pp. 40–49.

Translated by D. Voroshchuk